J|A|C|S
ARTICLES
Published on Web 11/22/2002

Effects of Surface Morphology on the Anchoring and Electrooptical Dynamics of Confined Nanoscale Liquid Crystalline Films

Alison R. Noble, Hye J. Kwon, and Ralph G. Nuzzo*

Contribution from the Department of Chemistry and the Frederick Seitz Materials Research Laboratory, University of Illinois at Urbana-Champaign, Urbana, Illinois 61801

Received July 22, 2002

Abstract: The orientation and dynamics of two 40-nm thick films of 4-*n*-pentyl-4′-cyanobiphenyl (5CB), a nematic liquid crystal, have been studied using step-scan Fourier transform infrared spectroscopy (FTIR). The films are confined in nanocavities bounded by an interdigitated electrode array (IDA) patterned on a zinc selenide (ZnSe) substrate. The effects of the ZnSe surface morphology (specifically, two variations of nanometer-scale corrugations obtained by mechanical polishing) on the initial ordering and reorientation dynamics of the electric-field-induced Freedericksz transition are presented here. The interaction of the 5CB with ZnSe surfaces bearing a spicular corrugation induces a homeotropic (surface normal) alignment of the film confined in the cavity. Alternately, when ZnSe is polished to generate fine grooves along the surface, a planar alignment is promoted in the liquid crystalline film. Time-resolved FTIR studies that enable the direct measurement of the rate constants for the electric-field-induced orientation and thermal relaxation reveal that the dynamic transitions of the two film structures are significantly different. These measurements quantitatively demonstrate the strong effects of surface morphology on the anchoring, order, and dynamics of liquid crystalline thin films.

Introduction

Insight into the molecular-level interactions that occur at interfaces is fundamental to the development of a wide range of materials technologies. Organic thin films in particular play a central role in such diverse areas as corrosion-inhibiting coatings,[1] the functioning of biological membranes,[2] transport and adsorbate binding in thin-film boundary layers,[3,4] and flat-screen displays.[5] This report describes the electrooptical properties and dynamics of thin liquid crystalline films, materials that are fundamental to the operation of liquid crystal (LC) displays.[5] An understanding of the thin film−substrate interactions that govern the dynamic transitions and surface binding (also called anchoring) of these materials, and the manner in which the physical properties of LC phase mediate these effects, is critical to the development of reliable, energy-efficient, and low-cost devices.[5]

The interactions of liquid crystals at cell boundaries have been examined in a number of leading studies.[6−12] Of significant interest in the context of this study is the recent work that describes the use of self-assembled monolayers (SAMs) as a molecular means to manipulate the anchoring interactions of liquid crystals.[13−17] These reports demonstrate that the tailoring of gold surfaces in this way can promote either planar or homeotropic alignment of simple nematic liquid crystalline phases. The work presented here is primarily concerned with the characteristics of ultrathin liquid crystalline films that experience interactions in the strong binding limit and the effects of surface morphology on the character of the thin film orientations and dynamics observed. We postulate that the influences of the nanometer-scale textures of our systems can operate in ways that are complementary with those seen in SAMs-based surface modifications.

Two confined film geometries are studied here: one in which the director is initially aligned in the surface normal, or homeotropic, direction; and a second that involves a higher symmetry alignment of the long axis of the 5CB planar to the substrate surface. An infrared (IR) cell of unique design is used to measure the electrooptical (EO) dynamic responses of these ultrathin liquid crystalline films.[18] As we will show, the

* Corresponding Author. Telephone: (217) 244-0809. Fax: (217) 244-2278. E-mail: r-nuzzo@uiuc.edu.

(1) Tallman, D. E.; Pae, Y.; Bierwagen, G. P. *Corrosion* **1999**, *55*, 779−786.
(2) Stuart, D. I.; Jones, Y. E. *Curr. Opin. Struct. Biol.* **1995**, *5*, 735−743.
(3) TeGrotenhuis, W. E.; Cameron, R. J.; Butcher, M. G.; Martin, P. M.; Wegeng, R. S. *Sep. Sci. Technol.* **1999**, *34*, 951−974.
(4) Guo, Y.; Colon, L. A. *Anal. Chem.* **1995**, *67*, 2511−2516.
(5) Goodman, L. A. *Introduction to Liquid Crystals*; Plenum: New York, 1995.
(6) Nakano, T.; Yokoyama, T.; Toriumi, H. *Appl. Spectrosc.* **1993**, *47*, 1354−1366.
(7) Kaito, A.; Wang, Y. K.; Hsu, S. L. *Anal. Chim. Acta* **1986**, *189*, 27−40.
(8) Ekgasit, S.; Fulleborn, M.; Siesler, H. W. *Vib. Spectrosc.* **1999**, *19*, 85−91.
(9) Gregoriou, V. G.; Chao, J. L.; Toriumi, H.; Palmer, R. *Chem. Phys. Lett.* **1991**, *179*, 491−496.
(10) Gregoriou, V. G.; Palmer, R. A. *Macromol. Symp.* **1995**, *94*, 75−95.
(11) Shilov, S. V.; Okretic, S.; Siesler, H. W. *Vib. Spectrosc.* **1995**, *9*, 57−63.
(12) Noble-Luginbuhl, A. R.; Blanchard, R. M.; Nuzzo, R. G. *J. Am. Chem. Soc.* **2000**, *122*, 3917−3926.
(13) Drawhorn, R. A.; Abbott, N. L. *J. Phys. Chem.* **1995**, *99*, 16511−16515.
(14) Gupta, V. K.; Abbott, N. L. *Langmuir* **1996**, *12*, 2587−2593.
(15) Gupta, V. K.; Miller, W. J.; Pike, C. L.; Abbott, N. L. *Chem. Mater.* **1996**, *8*, 1366−1369.
(16) Gupta, V. K.; Abbott, N. L. *Science* **1997**, *276*, 1533−1536.
(17) Miller, W. J.; Abbott, N. L.; Paul, J. D.; Prentiss, M. G. *Appl. Phys. Lett.* **1996**, *69*, 1852−1854.

10.1021/ja021001p CCC: $22.00

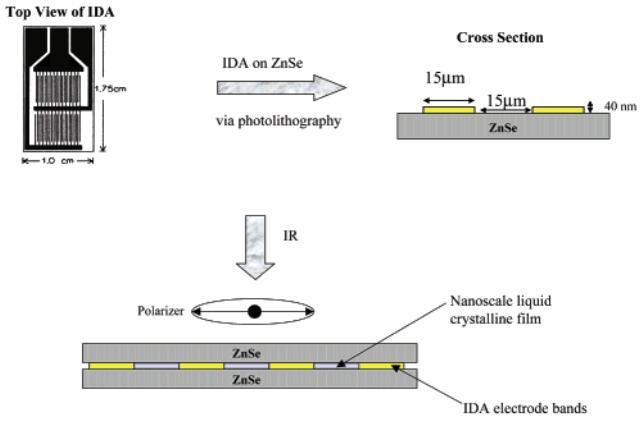

Figure 1. Configuration of IR cells. Shown are top and cross-sectional views of the interdigitated electrode array (IDA) patterned onto ZnSe. Electrode bands are 15 μm wide and 15 μm apart. Infrared radiation is incident in transmission geometry, and polarization directions (parallel and perpendicular) are defined relative to the electrode bands.

properties of these two films differ markedly, as demonstrated by the variations seen between the two films in both the orientation (here defined as the response of the liquid crystalline material upon the application of the field) and relaxation (the corresponding response seen after the removal of the field) dynamics. We discuss both the surface properties that induce the planar and homeotropic alignments and the profound effects of these organizational properties on the dynamics of these prototypical liquid crystalline thin films.

Experimental Methods

The design and fabrication of the IR cell used to confine the 40-nm thick films between the gold bands of an interdigitated electrode array (IDA) and the ZnSe substrate (patterned via photolithography) are described elsewhere.[12,18] In this study, two IR cells were constructed by patterning gold IDAs consisting of electrodes 15 μm wide and spaced 15 μm apart onto two ZnSe IR-transparent windows. The gold electrodes used in each case were 40 nm thick. A 1-μL drop of the liquid crystal 4-*n*-pentyl-4′-cyanobiphenyl (5CB) was placed onto the IDA pattern to ensure that all the cavities between the electrodes were filled. Unpatterned ZnSe windows were then placed on top of the filled IDAs, after which the assembled cells were compressed using metal weights to squeeze out any excess liquid crystal and to bring the top ZnSe windows into contact with the gold electrodes. The cells and weights were placed in an oven and heated overnight to 60 °C, a temperature well beyond the clearing point of this liquid crystal (35.3 °C), to facilitate the removal of excess liquid crystal from the cells. Confining the liquid crystals between the ZnSe windows and the electrodes in this way resulted in a confinement geometry that limits the thickness of the films to a height nominally defined by the electrodes (shown in Figure 1), in this case, 40 nm. It is important to note that, in filling the cells, it is likely that some 5CB became entrained between the top of the gold electrodes and the ZnSe crystals. This quantity appeared to be very small, perhaps on the order of a few monolayers, and did not have any experimentally demonstrable effect on the homogeneity of the electric field experienced by the molecules confined in the major portion of the EO cavity. Additionally, this material, if present, cannot contribute to the measured IR spectra because the data are collected in transmission mode, and the gold electrodes completely block the detection of spectra from these molecules.

The cells were fabricated and filled in a class 100 clean room to prevent airborne particulates (which can range on the order of several microns in size) from being caught in them and thus modifying the thickness of the confined layers. For FTIR measurements, each assembled cell was placed into a stainless steel sample holder, and the area surrounding the IDA pattern was masked off to ensure that the measured IR responses would be generated only from the electrode-bounded nanocavities. The instrument aperture was selected so as to probe the entire 1.0 × 0.30-cm^2 area patterned with electrodes.

After the initial filling of the cells with 5CB, a series of 15-V transients was applied repeatedly across the electrodes until the liquid crystals settled into a reproducible zero-field state. This processing is necessary to eliminate the hysteresis induced by the initial contact and spreading of the liquid crystals on the ZnSe surface.

Both rapid-scan and step-scan infrared measurements were made using a Bio-Rad (Cambridge, MA) FTS 6000 spectrometer equipped with a KBr beam splitter and a high-temperature ceramic source. A rotatable KRS-5 wire-grid polarizer was placed in the beam path to select IR radiation polarized in directions perpendicular and parallel to the IDA bands. Polarization directions are defined as shown in Figure 1. The data were collected using Win IR-Pro software designed specifically for use with the FTS 6000 spectrometer. The collected interferograms were single-sided (asymmetric), and a triangular apodization algorithm was used to weight the interferogram. For the rapid-scan experiments, data were collected with a deuterated triglycine sulfate (DTGS) detector at 4-cm^{-1} resolutions. The step-scan TRS (time-resolved spectroscopy) measurements were made using a liquid nitrogen cooled mercury cadmium telluride (MCT) detector equipped with a DC-coupled preamplifier.

This paper presents two distinct types of infrared measurement. The first probes systems that are held at static electrical polarizations, while the second is performed in conjunction with dynamic electrical polarizations. The measurements used to probe the systems while held at a constant potential were performed using rapid-scan acquisitions at an optical modulation of 5 kHz and a 1.2-kHz low-pass filter. For each spectrum, 32 scans were collected and averaged. The potentials applied across the cells were generated with a DC power supply with an output range from 0 to 15 V. Multiple ZnSe plates tend to generate strong interference fringes in infrared spectra, and as such, it is difficult to obtain artifact-free absolute spectra of the cells filled with 5CB (i.e., one ratioed to a background spectrum of an unfilled cell). For this reason, the data are reported as difference spectra (collected by referencing each scan to a single-beam scan of the filled cell held at 0 V).

Programmed electrical polarizations were applied across the cells for the collection of time-resolved spectra. These data were acquired at a scan rate of 5 Hz and a time resolution of 375 μs. Sixteen scans with a spectral resolution of 4 cm^{-1} were coadded. An optical long-pass filter was used, and the spectrometer was set to collect data at an undersampling ratio of 4 in order to limit the spectral range to 0−3950 cm^{-1}. Background scans were collected with the same setup, but with the cells disconnected from the voltage source.

Dynamic electrical polarizations were produced using a Wavetek function generator, programmed to apply square wave pulses of 12.3 V across the IDA for durations of 50 ms. These modulations were triggered to initiate and terminate the data collection during the step-scan experiments. Each pulse was applied at every mirror step after a settling time of 25 ms to allow the complete relaxation of the liquid crystals to their initial state before perturbation by the next pulse.

Results

The liquid crystal 5CB has a positive dielectric anisotropy.[19,20] It is this property that is exploited in the electric-field-induced reorientation of liquid crystals (also known as the Freedericksz

(18) Blanchard, R. M.; Noble-Luginbuhl, A. R.; Nuzzo, R. G. *Anal. Chem.* **2000**, *72*, 1365−1372.
(19) Ashford, A.; Constant, J.; Kirton, J.; Raynes, E. P. *Electron. Lett.* **1973**, *9*, 118−120.
(20) Gray, G. W.; Harrison, K. J.; Nash, J. A. *Electron. Lett.* **1973**, *9*, 130−131.

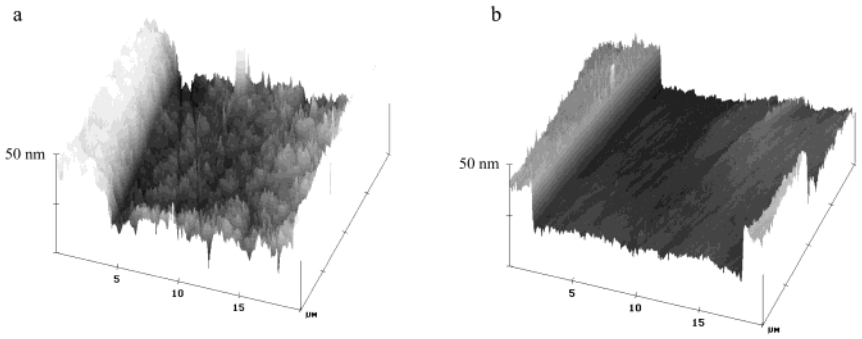

Figure 2. AFM micrographs of the (a) spicular and (b) grooved ZnSe substrates. Shown are the areas between two adjacent electrode bands.

transition).[19,21] When an electric field of sufficient magnitude ($V > V_{threshold}$) is applied across such a material, the molecules reorient so as to move the LC director (in this case, the average orientation of the long axis of the molecules) toward a direction that is parallel with the applied field. While the orientation of liquid crystals by an applied electric field has been extensively studied, most of the reports in the literature deal with films that are on the order of several microns thick. Additionally, the studies are performed in what is typically termed the "sandwich geometry." That is, the liquid crystals are confined between substrates which also serve as the electrodes; thus, the choice of substrate materials is typically confined to ones that are conducting.[6,22,23] Commonly used substrates for infrared studies include germanium and CaF_2 or BaF_2 coated with indium tin oxide (ITO).[6,9,10,23−25] In these experiments, the IR beam propagates in a direction that is parallel to the direction of the applied field and, as a result, limits the spectroscopic information that can be gained.

In this report, we detail the responses of ultrathin liquid crystalline films, ones only 40 nm thick, to electric field perturbations provided by an interdigitated array of band electrodes. As shown in previous work, this thickness is within the thin-film limit and the dynamics exhibit significant differences from those seen for more bulklike films.[12] In films of this thickness, the dynamics and organization of the molecules show marked perturbations that appear to originate from a complex interplay of surface and confinement effects. The results presented below develop this issue in detail and extend the observations made in an earlier report.[12] In the present research, the nanoscale electrooptical dynamics of two distinct LC organizational states are examined: one showing a homeotropic and the other a coplanar (parallel) alignment of the director. The organization in each case arises because of the effects of subtle nanoscale differences in the morphology of the cell surfaces that serve to confine the LC phase.

The experimental geometry employed in this study is illustrated schematically in Figure 1. This cell design consists of two sets of 50 pairs of interdigitated electrodes and two confining IR-transparent (but insulating) substrates. The IDA was photolithographically patterned onto the surface of one of the ZnSe windows. This fabrication process has been described in detail elsewhere.[18] For this study, we used electrodes that are 15 μm wide, 15 μm apart, and with a height of 40 nm, the last being the design rule that limits the dimension of the LC film. In this geometry, the propagation direction of the infrared radiation is oriented along a direction normal to the applied electric field. This allows the observation of changes in optical anisotropy over a wide range of optical polarization vectors, including the major axis lying parallel to the applied electric field.

Our studies follow earlier works that document the sensitivity of the nematic liquid crystalline phase to surface molecular structure and morphology.[26−32] Of particular interest because of its common use in display technology is the role played by polyimide alignment layers.[33] These films, when suitably rubbed, serve to control both the orientation and anchoring interactions of liquid crystals.[34,35] These effects originate from contributions made by both physical and molecular-level interactions occurring between the LC and polymer layer.[26,36] Generally speaking, the physical effect of interest to this study is the well-understood tendency of liquid crystals to orient either parallel to a grooved (or rubbing direction of a) surface or in a homeotropic orientation on one modified (by surfactants or other treatments) to present a more corrugated surface morphology.[26]

The two limiting ZnSe surfaces studied here are shown in the AFM micrographs presented in Figure 2. The scans are 20 μm wide and encompass the rising edges of two neighboring electrodes as well as a prototypical region of the ZnSe surface that contacts the 5CB. Both surfaces are corrugated with mean amplitudes on the order of a few nanometers; each texture was produced by mechanical polishing. The surface shown in Figure 2a induces homeotropic alignment of the liquid crystals, while that of Figure 2b promotes a 5CB alignment that is parallel to the surface and well aligned along the direction of the surface grooves. These alignments are demonstrated by the infrared data that are described immediately below.

(21) Freedericksz, V.; Repiewa, A. Z. *Z. Physik* **1927**, *42*, 352.
(22) Urano, T. I.; Hamaguchi, H. *Chem. Phys. Lett.* **1992**, *195*, 287−292.
(23) Toriumi, H.; Sugisawa, H.; Watanabe, H. *Jpn. J. Appl. Phys. Part 2* **1988**, *27*, L935−L937.
(24) Czarnecki, M. A.; Katayama, N.; Ozaki, Y.; Satoh, M.; Yoshio, K.; Watanabe, T.; Yanagi, T. *Appl. Spectrosc.* **1993**, *47*, 1382−1385.
(25) Shilov, S. V.; Skupin, H.; Kremer, F.; Gebhard, E.; Zentel, R. *Liq. Cryst.* **1997**, *22*, 203−210.
(26) Berreman, D. *Phys. Rev. Lett.* **1972**, *28*, 1683−1686.
(27) Janning, J. L. *Appl. Phys. Lett.* **1972**, *21*, 173−174.
(28) Blinov, L. M.; Chigrinov, V. G. *Electrooptic Effects in Liquid Crystal Materials*; Springer-Verlag: New York, 1994.
(29) Ong, H. L.; Hurd, A. J.; Meyer, R. B. *J. Appl. Phys.* **1985**, *57*, 186−192.
(30) Chaudhari, P.; Lacey, J.; Doyle, J.; Galligan, E.; Lien, S.-C. A.; Callegari, A.; Hougham, G.; Lang, N. D.; Andry, P. S.; John, R.; Yang, K.-H.; Lu, M.; Cai, C.; Speidell, J.; Purushothaman, S.; Ritsko, J.; Samant, M.; Stohr, J.; Nakagawa, Y.; Katoh, Y.; Saitoh, Y.; Sakai, K.; Satoh, H.; Odahara, S.; Nakano, H.; Nakagaki, J.; Shiota, Y. *Nature* **2001**, *411*, 56−59.
(31) Lee, B.-W.; Clark, N. A. *Science* **2001**, *291*, 2576−2580.
(32) Jerome, B. *Rep. Prog. Phys.* **1991**, *54*, 391−451.
(33) Kaneko, E. *Liquid Crystal TV Displays: Principles and Applications of Liquid Crystal Displays*; KTK Scientific Publishers: Tokyo, Japan, 1987.
(34) Paek, S.-H.; Durning, C. J. *J. Appl. Phys.* **1998**, *83*, 1270−1280.
(35) Newsome, C. J.; O'Neill, M.; Farley, R. J.; Bryan-Brown, G. P. *Appl. Phys. Lett.* **1998**, *72*, 2078−2080.
(36) Geary, J. M.; Goodby, J. W.; Kmetz, A. R.; Patel, J. S. *J. Appl. Phys.* **1987**, *62*, 4100−4108.

Table 1. Vibrational Mode Assignments for 5CB and the Angles of the Transition Moments Relative to the Long Axis of the Molecule

wavenumber (cm^{-1})			
lit[a]	obs	mode assignment	β[b] (deg)
3025	3025	phenyl C—H stretch	
2957	2957	methyl degenerate antisymmetric C—H stretch	
2926	2930	methylene antisymmetric C—H stretch	58.8
2870	2872	methyl symmetric C—H stretch	
2857	2857	methylene symmetric C—H stretch	59.2
2226	2226	C≡N stretch	20.0
1606	1606	phenyl C—C stretch	16.1
1494	1494	phenyl C—C stretch	15.5
1460	1466	C—H deformation of pentyl chain	
1397	1398	C—H deformation of pentyl chain	
1185	1185	phenyl C—H in-plane deformation	
1006	1006	phenyl C—H in-plane deformation, breathing	
818	814	phenyl C—H out-of-plane deformation	90

[a] References 9 and 22. [b] The angle between the transition moment direction and the molecular axis of the molecule. Reference 37.

The Electric Field-Dependent Responses of Homeotropic and Parallel Organizations of 5CB. The infrared mode assignments and corresponding transition moment directions of 5CB are given in Table 1. A series of difference spectra, measured as a function of the applied potential in two orthogonal polarizations, are shown in Figure 3. The polarization directions in which the data are collected are indexed to the IDA; in this coordinate system, the perpendicular polarization lies along the applied electric field lines, to which the parallel polarization is orthogonal. The data presented in Figure 3a are essentially identical to the ones that have been presented and discussed in detail in an earlier report.[12] They are reproduced here for the benefit of the reader in order to facilitate a comparison between the EO dynamics seen in the two organizational states. The significant nature of the differences evidenced in the two systems is well illustrated by the field-driven responses seen in these data.

The field-induced motions of 5CB change the net anisotropy of the LC medium by displacing the director from its initial equilibrium state. This effect can be easily understood in the context of the changes seen in the difference spectra shown in Figure 3. The C≡N stretch, which appears at 2226 cm^{-1}, lies nearly along the long axis of the molecule and is always a prominent positive feature in the difference spectra measured in the ⊥ direction. This arises trivially because of the fact that the field-induced motions always serve to increase the projection of this group along the applied field lines (and thus on the polarization vector of the data measured in the ⊥ direction). Alternately, the phenyl C—H out-of-plane deformation (814 cm^{-1}), whose transition moment lies at an angle nearly orthogonal to the long axis of the molecule, always appears as a negative intensity mode in the difference spectra when measured with similarly polarized light. The complex derivative-like line shapes seen in the C—H stretching region in these same spectra largely reflect the overlap of multiple modes with differing transition moment directions.

A simple picture emerges when one considers only the data shown in the upper panels of Figure 3a and b (those measured in the perpendicular direction). The applied electric field induces a reorganization of the 5CB director along that direction for each sample. The larger this applied field is, the larger the net displacement seen from the initial equilibrium value (both systems fully relax when the field is removed). How these changes in anisotropy are developed is markedly different in the two samples; this fact is clearly evidenced by even a casual examination of the data measured in the parallel (||) polarization direction. These latter data clearly establish that the initial organizations of the two LC films must differ significantly.

Figures 4a and b present a quantitative summary of the data shown in Figures 3a and b in the form of the voltage-dependent integrated peak areas of the C≡N stretching mode. When taken together, the data shown in these figures demonstrate that very different types of molecular motions accompany the field-induced alignments of the 5CB molecules in each case. The sample giving the data shown in Figure 3a (i.e., one with a spicular nanoscale texture at the cell boundary), for example, shows essentially no field response for data measured in the || direction (Figure 4a). The molecules that move in the field, then, must do so in ways that do not produce large changes in the projection of the various transition moments of 5CB on that polarization vector. The data presented in Figure 3b are quite different. The intensity changes seen in the ⊥ direction are inversely correlated with intensity changes seen in bands measured in the || direction (Figure 4b). These data can only be understood in the context of a model that presents the 5CB molecules in the two 40-nm cells in very different initial equilibrium organizations. For the cell based on the spicular ZnSe cell texture, the 5CB molecules must adopt a homeotropic alignment. This conclusion is fully supported by in-depth analyses presented in an earlier report from our laboratory.[12] The analysis of data for the second 5CB cell also imparts a simple model. The dichroism seen in Figures 3b and 4b can only be understood in the context of molecular motions of the long axes of the 5CB molecules that are dominantly constrained to projections lying on the planes defined by the ZnSe windows.

It is interesting to note that the nanoscale ridges seen in the AFM data (Figure 2b) run nearly along the axis defined by the IDA electrodes. We performed a separate measurement to determine whether these ridges, in cooperation with the IDA, produce a strong alignment of 5CB along that direction. To do this, we extracted from the 0-V single-beam spectra measured in the two polarizations the band due to the C≡N stretch of 5CB. Control experiments show that no interferences exist in this region, and the complex background is easily removed by a nonlinear baseline correction. This analysis allowed us to measure the net alignment of 5CB based on the dichroic ratio of the ν_{CN} mode, as given by $I(\|)_{CN}/I(\perp)_{CN}$. This value was found experimentally to be 2.1. A dichroic ratio in this range demonstrates that 5CB shows significant alignment in the cell along the coincident directions of the grooves and electrode fingers. We should note that this value is not a completely rigorous analysis of the net anisotropy; rather, it is a lower boundary. The reason for this is due to the fact that the polishing grooves are not completely aligned along the parallel optical axis used in making these measurements. Were the molecules to be somewhat canted, or even show splay in the aligned phase, both of these effects would serve to decrease the dichroism as measured earlier and thus serve to underestimate the actual net organization present.

A similar set of single-beam measurements of the $I(\|)_{CN}/I(\perp)_{CN}$ for the homeotropic sample does in fact show some net

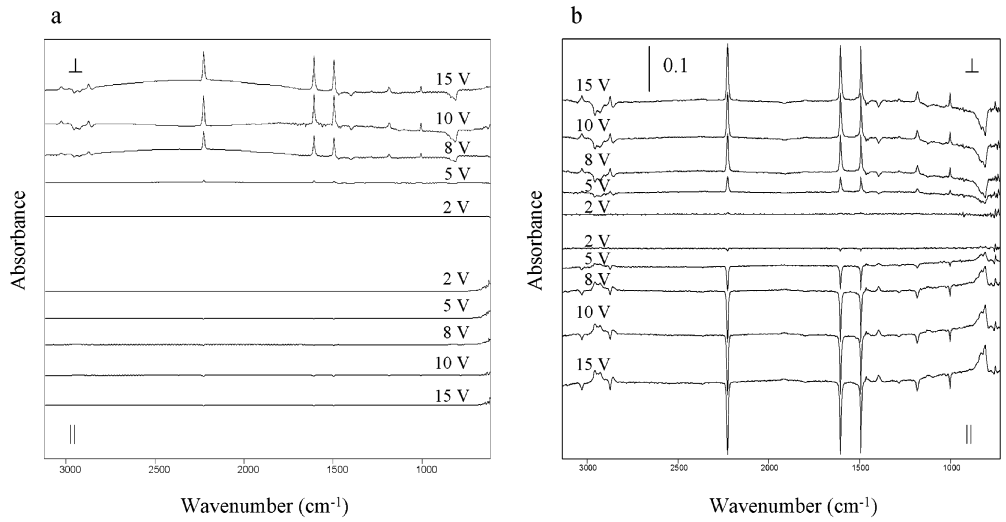

Figure 3. Stacked difference spectra of 40-nm films of 5CB at incrementally increasing potentials: (a) the homeotropic film on the spicular ZnSe substrate and (b) the planar film on the grooved ZnSe substrate. A reference spectrum is acquired at zero potential. The top panels show spectra acquired with IR light polarized in the perpendicular direction, and the bottom panels show spectra in the parallel polarization.

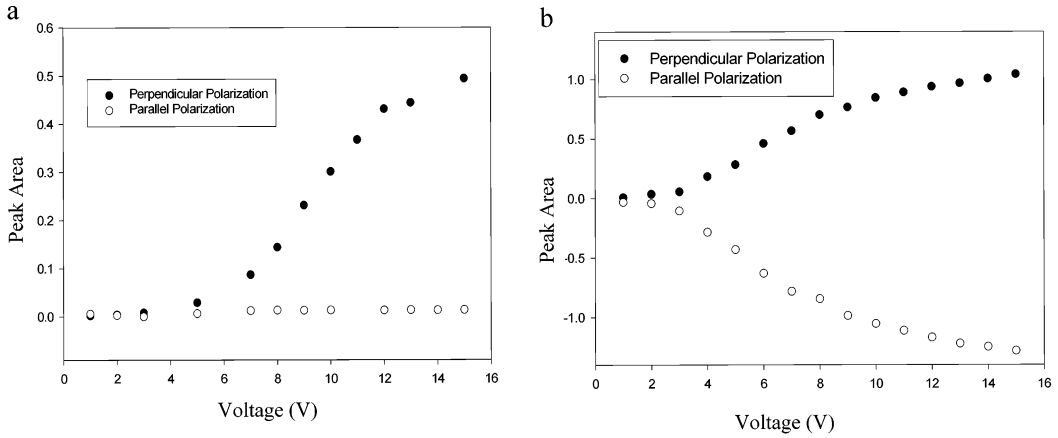

Figure 4. Integrated peak area versus applied voltage for the CN stretch at 2226 cm^{-1}: (a) spicular substrate (homeotropic film) and (b) grooved substrate (planar film).

projections of the ν_{CN} transition moment along both of these optical axes. The dichroic ratio measured in this way, 1.2, suggests that a weak preferential alignment exists along the || direction. We believe these latter results demonstrate that the average orientation of the 5CB molecules present in this phase is one that is canted off of the vector defined by the transverse cell direction. The dichroic ratio can only be understood then in terms of an organization that largely averages these cants over all azimuths. Taken together, the data clearly show that the electric field responses are extremely complex in that the alignment changes induced in this way do not equally perturb all the populations in this azimuthal average. Were it to do so, the spectra measured in the || direction would clearly show this, for example, in the form of holes appearing in the region of the ν_{CN} mode.

There are additional considerations that must be made to fully interpret the data measured on the 40-nm film supported on the grooved ZnSe substrate. As noted above, the electric-field-induced motions of 5CB are easily understood in the context of rotations of the molecular axes that are constrained to the plane of the electric field. The data show, however, that the intensity changes measured along the two optical axes are not exactly commensurate but are in fact slightly larger when measured in the parallel polarization direction. Figure 4b, which gives a quantitative description of this process in terms of the integrated peak areas for the C≡N stretching mode, demonstrates this anomaly as well. We can explain this behavior in the context of motions of 5CB that are constrained to a fully planar set of projections of the molecules. Their interpretation, however, requires a more in-depth analysis of the optical boundary values of this measurement, especially that relevant to the organizational anisotropy of the media. This analysis is detailed in the discussions provided in the Supporting Information.

It is useful here to consider the other correlations that follow from the alignments adopted by 5CB in these cells, as are suggested by our data. We find that the critical fields needed to drive measurable EO responses (Figure 4) are very different for the two 40-nm films. Specifically, the homeotropic alignment requires a critical field that is more than a factor of 2 larger in order to induce a measurable response (3333 vs 1333 V/cm). The homeotropic film also shows a more pronounced saturation of the response over the range of field strengths studied. These data suggest that greater energy is necessary to effect the Freedericksz transition and that this transition is much sharper in the homeotropic film than the parallel one. These facts are

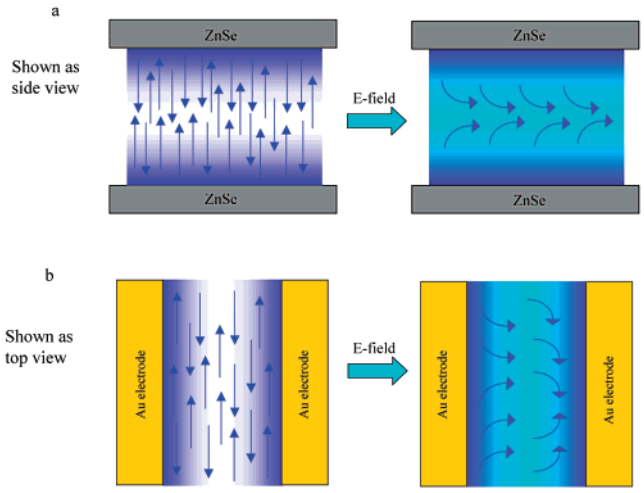

Figure 5. Schematic illustration of the initial alignments and electric-field-induced orientations of the two liquid crystalline films: (a) the homeotropic film (shown as a side view) and (b) the planar film (shown as a top view). The purple and blue colors are indicative of the surface and the electric field driving forces, respectively; the arrows approximate the orientations of molecules in bulk.

not surprising if we consider the properties expected for the planar and homeotropic films in some detail.

The applied electric field drives the bulk liquid crystalline molecules to reorient against the equilibrating force of the surface-bound molecules. As illustrated schematically in Figure 5, the reorientation effected by the field in our geometry is dominated in the planar film by a twisting motion of the bulk with respect to the surface-bound molecules, whereas the same field induces a bending and splaying motion in the bulk homeotropic film. When given that for bulk 5CB, K_{22} (the twist elastic constant; 3.9×10^{-12} N) is less than K_{11} (the splay elastic constant; 6.2×10^{-12} N) or K_{33} (the bend elastic constant; 8.9×10^{-12} N),[38] it is not difficult to surmise that the greater $V_{\text{threshold}}$ necessary to effect the Freedericksz transition in the homeotropic film results from a combination of the anisotropic properties of the liquid crystalline medium and the distinct alignments induced by the two surface morphologies. The twisting of bulk 5CB in the planar film has less energetic constraints, and thus low potentials are able to effect this movement; in the homeotropic film, the bending and splaying occur only if a field sufficiently strong to "buckle" the bulk liquid crystalline material is applied. The complexity of the motions revealed in this latter phase's field responses, however, precludes a more quantitative comparison via models formulated along the lines outlined later.

Time-Resolved Studies. The dynamics of the electric-field-induced motions were studied using step-scan infrared spectroscopy.[39−41] Unlike conventional FTIR spectroscopy, which uses only a single modulation frequency, the mirrors in the interferometer of a step-scan FTIR spectrometer move with a more complex set of modulation frequencies.[41] The step-scan interferometer modulates the mirror positions so that the optical retardation changes in a stepwise fashion. At each step, a programmed perturbation, in our case a square-wave pulse of fixed voltage applied to the IDA, is generated. Data are collected at each mirror retardation for the entire event. The entire set yields an array of data composed of one point measured at each mirror retardation and at each time. An interferogram can then be extrapolated for all times, which, upon Fourier transform, yields a three-dimensional data set of intensity versus wavenumber and time. Interferograms may also be extrapolated at any given time, down to the time resolution of the instrument, which for the purposes of this study was set to 375 μs. Time domain data for the homeotropic sample have been discussed in an earlier report.[12] Representative full, three-dimensional spectra measured in the perpendicular and parallel polarizations on the planar alignment sample are given in Supporting Information.

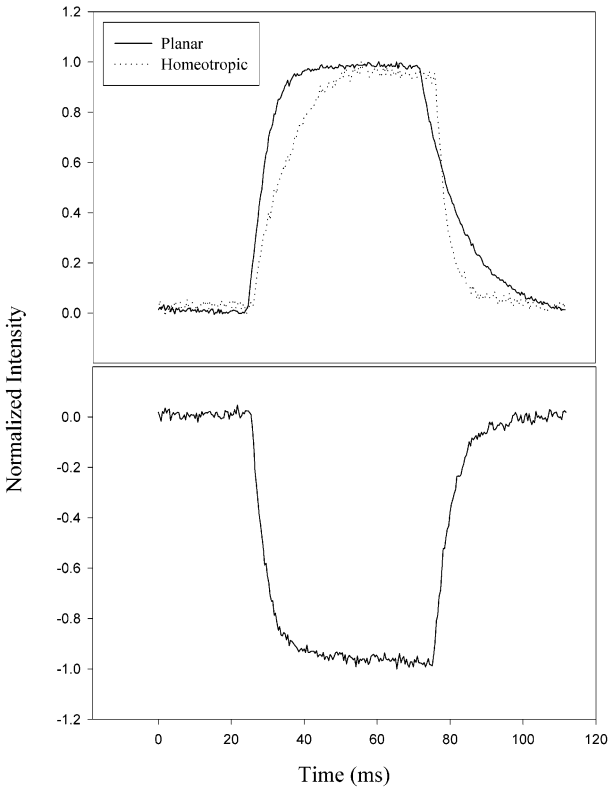

Figure 6. Temporal vibrational mode response (C≡N stretch; 2226 cm^{-1}) to an applied electric field square pulse in (a, upper panel) the perpendicular IR polarization for the homeotropic film and in both (a) the perpendicular and (b, lower panel) parallel polarizations for the planar film. The transients may be fit with exponential rise and decay functions to approximate the rate constants for the orientation and relaxation of 5CB.

Figures 6a and b show the $I_{\perp}$ and $I_{\parallel}$ responses of the 40-nm planar alignment film to 12.3-V square wave pulses, applied for a duration of 50 ms; Figure 6a also includes the $I_{\perp}$ response of the homeotropic film for comparison. The transients shown in the figure, measured specifically for the C≡N stretching mode centered at 2226 cm^{-1}, are extracted from the full data sets measured for the entire duration of the orientation and relaxation processes. The well-defined waveforms are representative of ones that can be extracted from other well-resolved vibrational modes of 5CB. The data may be interpreted by a model that treats the orientation and relaxation components of the complex waveform in the form of a single-exponential rate process. The orientation and relaxation rate constants (k_{or}, k_{rel}) calculated in

(37) Hatta, A. *Mol. Cryst. Liq. Cryst.* **1981**, *74*, 195−207.
(38) Dunmur, D. A. Measurements of Bulk Elastic Constants of Nematics. In *Physical Properties of Liquid Crystals: Nematics*; Dunmur, D. A., Fukuda, A., Luckhurst, G. R., Eds.; EMIS Datareviews Series No. 25; INSPEC: London, 2001; pp 216−229.
(39) Palmer, R. A.; Manning, C. J.; Pzepiela, J. A.; Widder, J. M.; Chao, J. L. *Appl. Spectrosc.* **1989**, *43*, 193−195.
(40) Manning, C. J.; Palmer, R. A.; Chao, J. *Rev. Sci. Instrum.* **1991**, *62*, 1219−1229.
(41) Crocombe, R. A.; Compton, S. V. *The Design, Performance and Applications of a Dynamically-Aligned Step-Scan Interferometer*, Bio-Rad Digilab Application Notes 82; Bio-Rad Digilab Division: Cambridge, MA, 1991.

Table 2. Rate Constants Calculated by a Single-Exponential Fit of Vibrational Mode Transients for the 40-nm Planar Film of 5CB in Two IR Polarizations

ν (cm^{-1})	k_{or}, $\perp$ (ms^{-1})	k_{rel}, $\perp$ (ms^{-1})	k_{or}, $\parallel$ (ms^{-1})	k_{rel}, $\parallel$ (ms^{-1})
1494	0.200 ± 0.003	0.0905 ± 0.0007	0.242 ± 0.005	0.215 ± 0.003
1606	0.199 ± 0.003	0.0905 ± 0.0007	0.240 ± 0.004	0.214 ± 0.004
2226	0.201 ± 0.003	0.0883 ± 0.0006	0.243 ± 0.003	0.204 ± 0.003

Table 3. Rate Constants Calculated by a Single-Exponential Fit of Order Parameters for the 40-nm Planar Film of 5CB, with Rate Constants of the Homeotropic Film for Comparison[a]

ν	planar orientation		homeotropic orientation[a]	
(cm^{-1})	k_{or}, S (ms^{-1})	k_{rel}, S (ms^{-1})	k_{or} (ms^{-1})	k_{rel} (ms^{-1})
1494	0.233 ± 0.003	0.0860 ± 0.0006	0.110 ± 0.003	0.2551 ± 0.0002
1606	0.231 ± 0.002	0.0882 ± 0.0006	0.106 ± 0.002	0.2556 ± 0.0002
2226	0.236 ± 0.002	0.0967 ± 0.0006	0.108 ± 0.002	0.2545 ± 0.0001

[a] Results reported previously in ref 12.

this way from waveforms extracted from representative modes are summarized in Tables 2 and 3. With regard to the homeotropic system, the two central points to note are the following: (a) the rates of the orientation and relaxation processes are markedly different (the latter are faster to a level that far exceeds the experimental uncertainty); and (b) the kinetic response is a completely homogeneous one in the sense that the time scales of importance are ones relevant to the complex fluid dynamics of 5CB, a time scale far longer than those associated with an individual molecule's segmental dynamics.

A qualitative comparison of the planar film's transients (Figure 6a and b) with that of the homeotropic alignment (Figure 6a) clearly demonstrates that the kinetics of the transitions differ significantly for the two films. The orientation of the homeotropic film occurs much more slowly than that of the planar film. Conversely, the relaxation process is much more rapid in the homeotropic film than that for the planar orientation film. This is consistent with the relative behaviors of the confined films elucidated by the static voltage measurements (recall that the threshold voltage required to initiate the transition was much larger for the homeotropic film). The observed trend is a direct result of the alignments induced by the distinct surface morphologies of ZnSe: the substrate texture, by inducing the initial equilibrium orientation of the liquid crystalline molecules, influences the orientation and relaxation dynamics (at least in part) by selecting the factors that become weighted (e.g., the specific bulk elastic constants) in the molecular mechanisms of the EO responses.

Our previous analyses of transients of the sort shown in Figure 6 were based upon single-exponential fits of the component orientation and relaxation processes.[12] The homeotropic film's data shown in Figure 6a can be fit well within the context of this simple exponential model; when taken separately, the planar film data for each polarization may be quantified similarly. The latter presents a new complication, however, which was not evidenced in the single polarization data accessible for the homeotropic case (see Figure 4a). The optical considerations of the planar 5CB film (Supporting Information) make it clear that a single-exponential fit to the data measured in either the (||) or ($\perp$) polarization directions cannot give a convergent assessment of the underlying rate behaviors. This arises from the fact that the intensity of the signal follows from more than

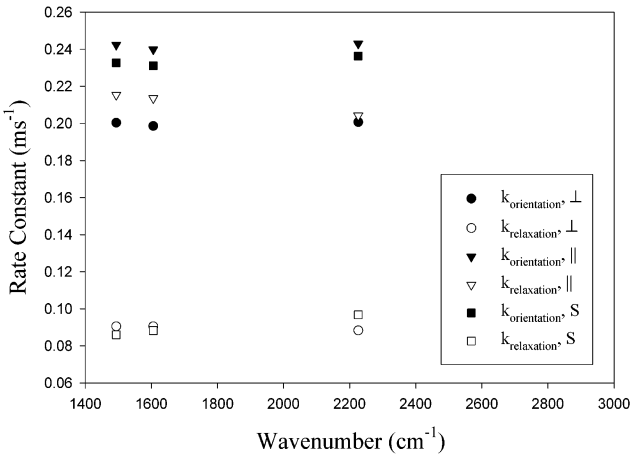

Figure 7. Rate constants calculated at 1494, 1606, and 2226 cm^{-1} for the orientation and relaxation processes. Also included for comparison are the rate constants calculated for the change in order parameter with time for the planar film.

just a consideration of simple mass action principles alone. In fact, the intensity of the rate transient depends not only on the change of the molecular orientation but also on the absolute initial orientation as well. Because of this effect, if the data were to be fit directly with single-exponential rate laws for the orientation and relaxation processes, a difference in the calculated rates of the two processes would be expected for identical processes measured in the different polarizations. Figure 7 and Table 2 summarize the rates of these two processes calculated in this way using waveforms extracted from representative vibrational modes of 5CB. The data measured in the perpendicular and parallel polarizations clearly yield different estimates of the relevant rate constants; the values from data measured in the parallel polarization are always larger. This result is clearly nonphysical and illustrates that a different model is necessary to fit these rate behaviors. A more rigorous way to describe the rate changes is in terms of the time-dependent evolution of the order parameter, S, of the liquid crystalline thin film.

The order parameter describes the level of anisotropy in a sample of liquid crystals and is given by the equation:[28]

$$S = \frac{1}{2}\langle 3\cos^2\theta - 1\rangle \tag{1}$$

where S is the order parameter and θ is the angle between the electric vector (polarization direction) and the long axis of the molecule. For a uniaxial system, it can be shown that[42]

$$S = \frac{1}{2}\langle 3\cos^2\theta - 1\rangle = \frac{A_{\parallel} - A_{\perp}}{A_{\parallel} + 2A_{\perp}} \tag{2}$$

where A is the absorption of the infrared radiation measured in the two indicated polarization directions. It follows, therefore, that the order parameter can also be described in terms of the dichroic ratio ($A_{\parallel}A_{\perp}$):

$$S = \frac{D-1}{D+2} \tag{3}$$

where D represents the dichroic ratio of the sample.

(42) Ward, J. M. *Adv. Polym. Sci.* **1985**, *66*, 81−115.

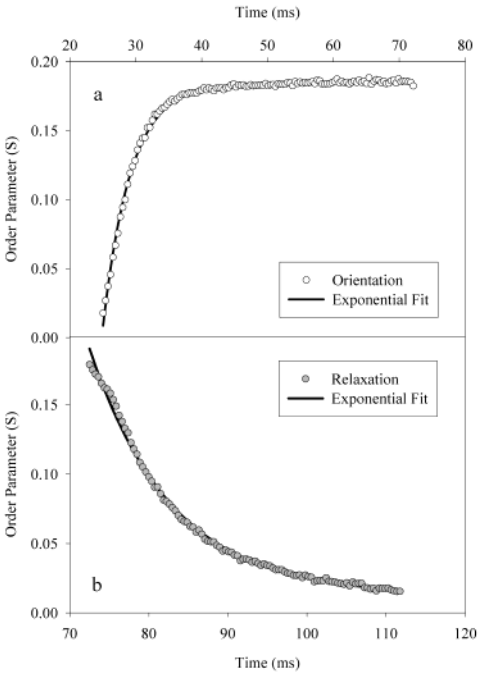

Figure 8. Exponential fits of the change in order parameter, *S*, at 2226 cm^{-1} for the planar film of 5CB: (a) single-exponential fit of the orientation in the electric field and (b) exponential decay fit of the relaxation after the removal of the field. Rate constants are listed in Table 2 and graphed in Figure 7.

The dichroic ratio, and thus the order parameter, of our planar sample can be calculated as a function of time. To do so, the initial absolute anisotropy is determined as described earlier, using single beam spectra acquired while the cell is held at zero potential. The time-resolved transients are then used to measure the change in absorbance as a function of time. The absolute dichroic ratio as a function of time may be calculated using the combination of the initial dichroic ratio and the change in absorbance over time. Finally, using eq 7, the order parameter of the thin film as a function of time can be calculated. Figure 8 shows the orientation and relaxation processes as described by the calculated time-resolved order parameter data along with their single-exponential fits. The rate constants calculated using the exponential fits of the order parameter as a function of time are listed in Table 3 and plotted in Figure 7. The order parameter fits lie fully within the limiting rate values calculated using the overly simplistic single-exponential model.

The homeotropic alignment cannot, of course, be analyzed in this way because the motions occurring in the transverse direction are not accessible to direct experimental observation. Even so, it remains likely that the single-exponential fit correctly captures the relative divergences of the orientation and relaxation rates. We also believe, given the magnitude of the perturbation used here (a weak one that is still probing a largely linear system response), that the quantitative differences seen in comparison with the planar system are also very good approximations of how the dynamics differ in these two cases. It is very interesting to note the systematic trends evidenced in this estimation of the rate behaviors and the property differences seen between the two confined films. The rate constant for the orientation of the homeotropic film is much smaller than that for the planar film; the collective field-induced motions of the 5CB occur much more rapidly for the planar film than for the homeotropic

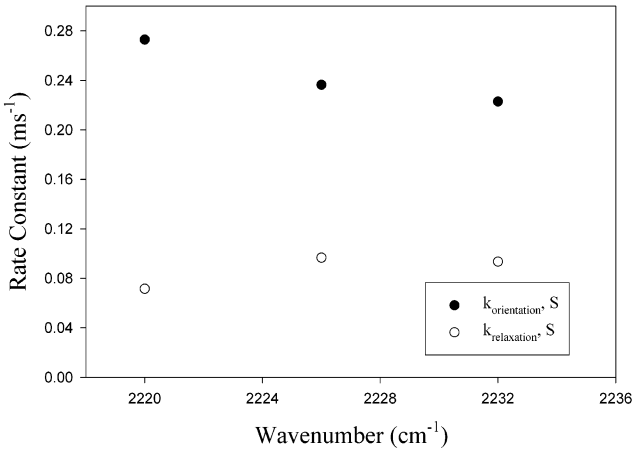

Figure 9. Rate constants measured across the width of the CN vibrational mode. Shown are data for the orientation and relaxation transients at 2220, 2226, and 2232 cm^{-1}.

film. The relaxation processes show the opposite trend: the rate constant for the homeotropic film is much larger than for the planar film, indicating that the molecules in the homeotropic film take much less time to return to the lower energy configuration of the initial equilibrium state. It is clear from this simple quantitative description that the rates of orientation and relaxation for the two films are fundamentally different, but in a way that may be predicted from considering the molecular mechanisms of the transitions and the bulk elastic constants of the medium. Thus, in directing the initial orientation of 5CB, the surface morphologies also impact the dynamic responses of the films by selecting the dominant features contributing to the transition mechanisms, as depicted schematically in Figure 5.

One additional point of consideration is relevant to this comparison. In an earlier study of confinement effects on EO dynamics, we examined the kinetic homogeneity of the response of a 40-nm homeotropic system in a very different context than the mode-by-mode comparison discussed earlier. In the aforementioned analysis, time slices were extracted from a specific vibrational band (the ν_{CN} mode) measured across the extent of its presumably heterogeneously broadened line width. In thicker films (300 nm), the lower frequency side of the band masked contributions from fast population responses present only in the orientation dynamics (i.e., the field driven response). These fast domain responses were not seen in the data measured on the 40-nm sample. We interpreted this phenomenon as suggesting a natural correlation length in the problem, one that delimits a transition of the system toward more bulklike properties. This confinement limit need not be the same for the very different organization of the planar alignment.

Figure 9 shows a plot of the rate constants obtained from exponential fits of the order parameters calculated from waveforms extracted from time slices taken across the width of the ν_{CN} mode, which, on the basis of our previously established precedent, sensitively reports on the local details of the heterogeneity present in the sample. The data in the figure indicate that small divergences exist in the measured kinetics of both the orientation and relaxation processes that lie outside the limits imposed by the experimental uncertainty. The differences observed in the lower frequency side of the band, though, are not as significant as those seen in the 300-nm

homeotropic film. As a result, we cannot unequivocally interpret these data as signifying similar correlation length sensitivity in the current planar sample. One point to note in this system, however, is that the limiting dimension of 40 nm in the planar case confines the liquid crystal molecules less stiffly than in the homeotropic system, since the molecules lie down on the ZnSe surface instead of standing end-to-end. We postulate that this property likely imparts a more bulklike quality to the planar 40-nm system, including the similarity of its dynamics to those measured for the thicker 300-nm homeotropic film. This correlates well with the softened, yet still notable, presence of fast field response components being weighted in the low-frequency side of the ν_{CN} mode. The current system thus displays a unique profile for the confinement effects operating on a film with a planar organization.

Discussion

The data presented above develop an interesting set of correlations regarding the sensitivities of the organizational structures and the electrooptical dynamics of ultrathin liquid crystalline films to surface morphology. The surface clearly directs thermodynamically the structures of the liquid crystalline phases, since the field-driven changes always relax back to their initial state. In directing the equilibrium alignment, the substrate morphology also significantly, albeit indirectly, impacts the dynamic responses of these confined thin films to the influences of external fields. Embedded in the dynamic data are the mechanisms of molecular movement and their relevant energetic considerations. These follow simply from the analyses presented above: the electric-field-effected reorientation process in the homeotropic case is dominated by bending and splaying motions (and their corresponding elastic constants), while twisting motions (and its elastic constant) figure more heavily in the reorientation of the planar film.

The structures of the two types of 5CB films examined here are anisotropic in ways that follow quite sensibly from the structural characteristics of the substrates that induce their alignment. In both cases, the organizations are induced by remarkably fine substrate textures, involving, on average, nanometer-scale corrugations. It is unlikely that secondary issues related to the interfacial interactions are involved here, since, in each case, an identical set of chemical interactions is involved. Our XPS data, for example, have shown that the surfaces contacting these liquid crystalline phases essentially consist of ZnO (the near surface region of the ZnSe is enriched in this oxide). Imaging XPS data also reveal that the photoresist processing, when carried out appropriately, does not leave molecular residues that might then act as an alignment layer. The differences in the alignments seen between the two systems thus appear to relate simply to the energy costs of elastic strains.

In the case of the homeotropic film, one might speculate analogously with previous works that a surface-induced short-range smectic A ordering exists near the surface. Such ordering of nematic liquid crystals has been observed experimentally and results in an apparent increase in the surface potential.[28,43,44] This does not seem likely in our view because the rough texture of this surface should frustrate any such smectic ordering; the cases examined in earlier works employed extremely smooth surfaces. The critical factors to consider in the ordering of these liquid crystalline phases then seem to be (a) the imposition of a finite confinement geometry and (b) nanometer-scale substrate textures that the ZnSe presents to the films.

The 40-nm limiting confinement dimension provides a strong perturbation that should promote the adoption of a planar organization of the 5CB.[26] The IDA electrodes, but more importantly the groove-like textures present on the substrate, provide an additional bias that must serve to generate the anisotropy of the alignment seen in the planar sample. The point of interest, then, is the factor that serves to drive the liquid crystalline molecules to adopt the homeotropic alignment; the nanometer-scale spicular texture must clearly induce this organization. The one-dimensional order present in a nematic phase can accommodate this texture with little energy cost by aligning its long axis along the surface normal direction. Any other orientation of the nematic phase would increase strains and unfavorable boundary interactions as the nematic fluid deforms to accommodate the high-aspect-ratio features of this cell's surfaces. The structural outcome seen for the ridged corrugation is less problematic to rationalize, since well-understood precedents for the planar alignments induced by similar surface morphologies have been established in the literature.[26,28,30,45]

Perhaps the most interesting observation to emerge from this work is the fact that the dynamics of the field-induced orientation and thermal relaxation show significant divergences. The two rates are markedly different for the homeotropically aligned 5CB film, with a faster relaxation process than orientation being seen; the planar film also displays a similar disparity of the two rates, but with a reversed trend. The differences observed in the rate constants are clearly a result of the alignment geometries induced by the substrate textures and operate via the distinct molecular motions of the liquid crystalline molecules in the two phases.

The time scales of the orientation and relaxation rate constants themselves (on the order of milliseconds) are, in one sense, all quite similar and fall in a range of the order as might be expected in a bulk phase of 5CB.[46] Since the response of the liquid crystalline phase to an external field presumably involves the motions of fluid domains, this bounding limit of the relevant time scales is not surprising. It is remarkable, however, that while the rates seen in our experiments are limited in magnitude by the bulk fluid properties of 5CB, they show pronounced sensitivities to the organizational anisotropy of the phase, the elastic properties of the medium, and (although not quantitatively developed in detail here) the degree and character of the deformation induced by the field. In a forthcoming publication, we will show that all these sensitivities can be accounted for quantitatively in theory.[46]

A significant point of consideration, as yet untouched in this discussion, is how the imposed confinement dimension impacts the fluid properties and the new effects it might have on the dynamics. Two relevant factors that appear to be most influenced by the confinement limit are the domain shapes and the frictional interactions between the field-driven domain motions. Unfortunately, the present data do not address themselves to either

(43) Horn, R. G.; Israelachvili, J. N.; Perez, E. *J. Phys. (Paris)* **1981**, *42*, 39−52.
(44) Rosenblatt, C. *Phys. Rev. Lett.* **1984**, *53*, 791−794.
(45) Collings, P. J. *Liquid Crystals: Natures Delicate Phase of Matter*; Princeton University Press: Princeton, NJ, 1990.
(46) Kwon, H. J.; Schweizer, K. S.; Nuzzo, R. G. To be submitted for publication.

of these issues in a quantitative way. We note, however, that our data suggest that the responses measured for the 40-nm cells are more kinetically homogeneous. The thicker homeotropic film of previous experiments exhibited more heterogeneous kinetics in the field-driven responses;[12] thinner cells appear to lead to more homogeneous and perhaps coherent behaviors. Interestingly, the inherent correlation lengths of nematic domains, typically a few hundred angstroms,[47] well approximate the 40-nm limiting dimension adopted in this study and may hint at the underlying structure of the liquid crystalline domains. Further experimental work will be needed to clarify this issue.

When taken together, the results of this study demonstrate that the physical texture of substrate materials can have a significant impact not only on the organizational properties of a liquid crystalline phase but also on the quantitative details of its electrooptical dynamics. The influences of the confinement appear to amplify these effects, presumably via the operation of biases that drive a more coherent response and provide for a larger sample-weighted impact of the effects contributed by the contacting interfaces of the cell.

We close this discussion by noting that the experiments reported in this study, while informative, suffer from a considerable limitation. One point of concern is the somewhat arbitrary characteristic of the major experimental determinant: a surface texture that is difficult to control and that offers limited prospects for a rational molecular design. Clearly, the dynamics seen in the homeotropic alignment would be the most difficult to model, given the complexity of the elastic deformations involved in its electrooptical responses. Such complex cooperative behaviors may never be accessible to a full theoretical description. It seems likely that the types of motions that move the director in the planar film, and the forces that mediate them, are more tractable models for further quantitative study. A liquid crystalline cell with planar alignment and motions is also more technologically relevant because of its inherent advantages (e.g., wider viewing angle)[48] and is more easily manipulated with surface treatments.

The limitations not withstanding, these studies illustrate the experimental directions that must be taken to refine the novel measurements reported here to enable the collection of data appropriate for guiding the construction and critical testing of a full theoretical description of this fascinating example of nanoscale dynamics. In a future report, we will describe a revised cell design that simplifies and molecularly rationalizes the cell/LC contact boundary interactions. The data obtained with this device appear well suited to critically test and provide detailed experimental confirmations of a comprehensive new theory of the dynamics.[46]

Acknowledgment. We gratefully thank the National Science Foundation (NSF CHE 00-97096) and the Department of Energy (DEFG02-91ER45439) for their support of this work and the Defense Advanced Research Projects Agency for providing funds used to purchase the spectrometer. AFM and XPS studies were carried out at the Center for Microanalysis of Materials at the University of Illinois at Urbana-Champaign, supported by the Department of Energy under Contract DEFG02-91ER45439.

Supporting Information Available: Analysis of the optics of the spectroscopic measurements and complete three-dimensional time-resolved FTIR spectra (750−3100 cm^{-1}) from step-scan experiments in both the perpendicular and parallel polarizations for the planar film. This material is available free of charge via the Internet at http://pubs.acs.org.

JA021001P

(47) DeGennes, P. G.; Prost, J. *The Physics of Liquid Crystals*; Clarendon: Oxford, 1993.

(48) Oh-E, M.; Kondo, K. *Liq. Cryst.* **1997**, *22*, 379−390.